AIAA 2003–3400

CFD Sensitivity Analysis of a Drag Prediction Workshop Wing/Body Transport Configuration

E. M. Lee-Rausch
P. G. Buning
J. H. Morrison
M. A. Park
S. M. Rivers
C. L. Rumsey
NASA Langley Research Center
Hampton, Virginia

D. Mavriplis
National Institute of Aerospace
Hampton, Virginia

21st AIAA Applied Aerodynamics Conference
June 23–26, 2003
Orlando, FL

CFD Sensitivity Analysis of a Drag Prediction Workshop Wing/Body Transport Configuration

E. M. Lee-Rausch * P. G. Buning † D. Mavriplis ‡ J. H. Morrison §
M. A. Park ¶ S. M. Rivers ‖ C. L. Rumsey **

Abstract

The current work re-visits calculations for the First AIAA Drag Prediction Workshop (DPW-I) configuration and uses a grid convergence study to evaluate the quantitative effects of discretization error on the code-to-code variation of forces and moments. Four CFD codes commonly used at NASA Langley Research Center are used in the study: CFL3D and OVERFLOW are structured grid codes, and NSU3D and FUN3D are unstructured grid codes. Although the drag variation reported in the summary of DPW-I results was for the constant-lift cruise condition, the focus of the current grid convergence study is a constant angle-of-attack condition ($\alpha = 0^\circ$) near the same cruise lift in order to maintain identical boundary conditions for all of the CFD codes. Forces and moments were computed on the standard DPW-I structured overset and node-based unstructured grids, and the results were compared for the required transonic drag polar case. The range in total drag predicted using the workshop standard grids at $\alpha = 0^\circ$ was 14 counts. The variation of drag in terms of standard deviation was 6 counts. Additional calculations at $\alpha = 0^\circ$ were performed on the two families of structured and unstructured grids to evaluate the variation in forces and moments with grid refinement. The structured grid refinement study was inconclusive because of difficulties computing on the fine grid. The grid refinement study for the unstructured grid codes showed an increase in variation of forces and moments with grid refinement. However, all of the unstructured grid results were not definitively in the range of asymptotic grid convergence. The study indicated that certain numerical schemes (central vs. upwind, thin-layer vs. full viscous) or other code-to-code differences may have a larger effect than previously thought on grid sizes considered to be "medium" or "fine" by current standards.

*Member AIAA, Research Engineer NASA Langley Research Center(LaRC), Hampton, Virginia.
†Associate Fellow AIAA, Senior Research Scientist NASA LaRC.
‡Associate Fellow AIAA, Research Fellow National Institute of Aerospace, Hampton, Virginia.
§Senior Member AIAA, Research Scientist NASA LaRC.
¶Member AIAA, Research Engineer NASA LaRC.
‖Member AIAA, Research Scientist NASA LaRC.
**Associate Fellow AIAA, Senior Research Scientist NASA LaRC.

Introduction

The AIAA Applied Aerodynamics Technical Committee conducted a Drag Prediction Workshop (DPW-I) in the summer of 2001 to evaluate CFD transonic cruise drag predictions for subsonic transports. Workshop participants were required to calculate the lift, drag and pitching moment for the DLR-F4 wing-body configuration at the cruise condition (Mach = 0.75, C_L = 0.5), as well as the Mach = 0.75 drag polar. The participants were given a required grid to run and were encouraged to develop their own grid. The DLR-F4 wing-body was chosen since it had been tested in multiple wind tunnels.[1]

A total of 35 solutions were computed with 14 different CFD codes; multiple turbulence models were used; structured and unstructured grids were used; 21 solutions were submitted on the required grids and an additional 14 solutions were provided on grids developed by the participants. In Ref. 2, Levy et al. provided a description of the workshop requirements and summary of the data submitted by the workshop participants. Hemsch[3] analyzed all of the solutions using a statistical framework. The variation in the drag from all 35 solutions at the cruise condition as measured by an estimate of the population standard deviation was 0.0021. The variation in the drag from the experiment was 0.0004. Thus, the computational drag variation was over 5 times the variation between wind tunnels. Designers typically state that they require drag prediction within one count (one count = 0.0001). Thus, the wind tunnel variation was 4 times the designer's requirement, and the CFD variation was 21 times the designer's requirement.

Roache[4] stated that multiple grids must always be used in order to verify a CFD solution. The design of the first DPW-I did not require that the participants provide solutions on multiple grids. Hence, the solutions were evaluated in the original study without the benefit of a quantitative measure of grid convergence. Each participant was free to choose whichever turbulence model and numerical scheme that they preferred for their calculations. Additionally, in order to accommodate the maximum number of CFD codes possible, the transition was specified at the leading edge of the vehicle, i.e. fully turbulent, rather than matching the experimentally determined transition pattern. Also, although aeroelastic deformations were incorporated into the geometry, they

were determined for a specific loading condition.

Some DPW-I participants published detailed results from their contributions to the workshop. Rakowitz et al.[5] presented multi-block structured grid results from the FLOWer code and hybrid unstructured grid results from the TAU code. Additionally, they investigated the effects of artificial dissipation, grid topology, grid quality, geometry modeling as well as global grid refinement on the structured grid and grid adaptation on the unstructured grid. This parameter study failed to account for the variation noted in Ref. 5 between the unstructured grid results and both the structured grid results and the experimental results. Mavriplis and Levy[6] presented hybrid grid results from the NSU3D code and investigated trailing-edge grid refinement and global grid h-refinement. Pirzadeh and Frink[7] presented tetrahedral unstructured grid results from the USM3Dns code with wall functions and compared the computational data to the workshop statistical analysis of Hemsch.[3] Rumsey and Biedron[8] presented multi-block structured grid results for CFL3D and studied the effects of grid quality/resolution, turbulence models, and transition. They noted that in comparison with the structured overset grid, the workshop 1-to-1 multi-block structured grid was too coarse to resolve the surface pressures and of overall poor quality. Vassberg, Buning, and Rumsey[9] presented structured overset grid results from the OVERFLOW code and provided a detailed comparison and analysis of the experimental data. The OVERFLOW drag prediction was compared to CFL3D overset grid results at the design point.

In the study of a different transport configuration, Rumsey et al.[10] provided an analysis of different effects on the prediction of lift, drag and pitching moment using CFL3D and OVERFLOW. They evaluated the effects due to turbulence model, grid refinement, outer boundary location, aeroelastic deflection, and numerical differencing. Their results showed that the turbulence model was the largest effect once a sufficiently refined grid was achieved.

The current work re-visits the DPW-I calculations for the DLR-F4 wing-body and uses a grid convergence study to evaluate the quantitative effects of discretization error on the code-to-code variation of forces and moments. Four CFD codes commonly used at NASA Langley Research Center are used in the study: CFL3D,[11] OVERFLOW,[12] NSU3D[13] and FUN3D.[14] In the current work, the effects of grid density on the variation of forces and moments is assessed for all four of the codes. Results from CFL3D, OVERFLOW and NSU3D were submitted to the first DPW,[2,6,9] but only NSU3D conducted a grid density study for the workshop. However, the h-refinement strategy used by Mavriplis in Ref. 6 did not project the newly created surface points to the original geometry so the results will not be included in this grid convergence study. Note that most of the CFL3D results for the original workshop were on block structured 1-to-1 grids. In the current work, additional cases were computed using CFL3D on overset grids, and the only structured grid results shown (using either CFL3D or OVERFLOW) are for overset grids. Although the drag variation reported in the summary of DPW-I results[2] was for the constant-lift cruise condition ($C_L = 0.5$), the focus of the current grid convergence study is a constant angle-of-attack condition ($\alpha = 0^\circ$) near the same cruise lift in order to maintain identical boundary conditions for all of the CFD codes.

Test Configuration and Data

In this computational study, we use the DLR-F4 wing-body configuration, as employed for the First AIAA Drag Prediction Workshop[2] for transonic drag prediction. The DLR-F4 is typical of a modern subsonic transport aircraft, and there is an extensive experimental and computational database available for this configuration. The DLR-F4 wing-body was tested in three different wind tunnels. The experimental data is documented in Refs. 1 and 15. A summary of computational results from the Drag Prediction Workshop is available.[2] A statistical analysis of the CFD solutions from the workshop is also available.[3]

Flow Solvers

Four Reynolds averaged Navier-Stokes (RANS) CFD codes are employed in this study: CFL3D and OVERFLOW are structured grid codes, and NSU3D and FUN3D are unstructured grid codes.

Structured Grid Codes

CFL3D and OVERFLOW are multi-zone codes which can use overset grids. Both employ local time-step scaling, grid sequencing and multi-grid to accelerate convergence to steady stage. A time-accurate mode is available for each code, and both can employ low-Mach number preconditioning for accuracy in computing low-speed steady-state flows.

CFL3D[11] is a cell-centered finite-volume method. It uses third-order upwind-biased spatial differencing on the convective and pressure terms, and second-order differencing on the viscous terms; it is globally second-order accurate. Roe's flux difference-splitting (FDS) method[16] is used to obtain fluxes at the cell faces. The solution is advanced in time with an implicit three-factor approximate factorization method. CFL3D has the capability to use the thin-layer approximation in any combination of the three coordinate directions (in other words, if thin-layer is employed in all three directions then the result is full Navier-Stokes without cross-derivative

terms). Thin-layer viscous terms are computed in wall-normal directions by default; additional viscous thin-layer terms are included in some calculations as noted.

OVERFLOW[12,17] is a structured (overset grid) Navier-Stokes flow solver. It uses a finite-difference formulation, with flow quantities stored at the grid vertices. OVERFLOW has central- and Roe upwind-difference options, and uses a diagonalized, implicit approximate factorization scheme for the time advance. In this study as in previous DPW-I results,[9] 2nd-order central differencing with Jameson-type 2nd/4th-order scalar dissipation[18] is used except as noted. Thin-layer viscous terms are computed in wall-normal directions by default; additional viscous thin-layer and cross-derivative terms are included in some calculations as noted.

For this study, both codes employed PEGASUS 5 software (Suhs et al.[19]) to obtain overset interpolants for the regions of overlapping grid.

Unstructured Grid Codes

NSU3D and FUN3D are finite-volume methods in which the flow variables are stored at the vertices of the mesh. NSU3D solves the equations on mixed element grids including tetrahedra, pyramids, prisms, and hexahedra while FUN3D is currently limited to tetrahedra only for turbulent flows.

FUN3D[14,20,21] employs an implicit upwind algorithm in which the inviscid fluxes are obtained with a flux-difference-splitting scheme and the viscous terms are evaluated with a finite-volume formulation, which is equivalent to a Galerkin type of approximation for these terms. There are no thin-layer approximations for the viscous terms. At interfaces delimiting neighboring control volumes, the inviscid fluxes are computed using a Roe Riemann solver based on the values on either side of the interface. For second-order accuracy, interface values are obtained by extrapolation of the control volume centroidal values, based on gradients computed at the mesh vertices using an unweighted least-squares technique. The solution at each time-step is updated with a backwards Euler time-differencing scheme. At each time step, the linear system of equations is approximately solved with either a point implicit procedure or an implicit line relaxation scheme.[22] Local time-step scaling is employed to accelerate convergence to steady-state.

NSU3D[13] includes two options for the discretization of the inviscid convective terms. The first option employs a Roe-Riemann solver at control volume interfaces, with a least squares gradient reconstruction procedure for second-order accuracy, similar to the FUN3D discretization. The second option employs centrally differenced convective terms with added matrix-based artificial dissipation. Second-order accuracy is achieved by formulating these dissipative terms as an undivided bi-harmonic operator, which is constructed as two passes of a nearest neighbor Laplacian operator. In the matrix form, this dissipation is similar to that produced by the Riemann solver gradient based reconstruction technique, and is obtained by replacing the difference in the reconstructed states on each side of the control volume interface by the undivided differences along mesh edges resulting from the biharmonic operator construction. In both cases, these differences are then multiplied by the characteristic matrix to obtain the final dissipative terms. The matrix dissipation formulation is used exclusively in this study. The thin-layer form of the Navier-Stokes equations is employed in all cases, and the viscous terms are discretized to second-order accuracy by finite-difference approximation. The basic time-stepping scheme is a three-stage explicit multistage scheme. Convergence is accelerated by a local block-Jacobi preconditioner in regions of isotropic grid cells. In boundary layer regions, where the grid is highly stretched, a line preconditioner is employed.[23] An agglomeration multigrid algorithm is used to further enhance convergence to steady-state.

Turbulence Model

For the current study, the one-equation turbulence model of Spalart and Allmaras is used.[24] CFL3D, NSU3D and FUN3D employ the version of SA referred to as SA-Ia. This is the version of the model that is given in Spalart and Allmaras,[24] and will be referred to simply as "SA" from now on. There is also a version of SA in wide use that is unpublished: it employs an additional term f_{v3} that multiplies part of the source term. This unpublished version will be referred to as "SA+fv3". OVERFLOW by default employs SA+fv3, although the capability to use SA has recently been added to the code. For all the results in the current study, OVERFLOW with SA+fv3 was employed. The differences between SA and SA+fv3 can be summarized as follows (refer to Spalart and Allmaras[24] for the form of the transport equation):
Version SA:

$$\hat{S} = \Omega + \frac{\hat{\nu} f_{v2}}{\kappa^2 d^2} \tag{1}$$

$$f_{v2} = 1 - \frac{\chi}{1 + \chi f_{v1}} \tag{2}$$

Version SA+fv3:

$$\hat{S} = f_{v3}\Omega + \frac{\hat{\nu} f_{v2}}{\kappa^2 d^2} \tag{3}$$

$$f_{v2} = \frac{1}{(1 + \chi/C_{v2})^3} \tag{4}$$

$$f_{v3} = \frac{(1 + \chi f_{v1})(1 - f_{v2})}{\chi} \tag{5}$$

The unpublished SA+fv3 model tends to delay boundary-layer transition relative to SA at moderately

low Reynolds numbers (e.g., 1 to 10 million), even when the model is turned on everywhere ("fully turbulent"). At higher Reynolds numbers, the differences between the two versions are less significant. Rumsey et al.[8] provided an analysis of the effects on the prediction of lift, drag and pitching moment of this variation in the SA turbulence model for the DPW-I standard block structured 1-to-1 grid. Their results showed that the overall effect of the SA+fv3 was small in the integrated quantities. The difference was 1.8% in lift, 3.3% in moment and 0.4% in drag.

Computational Grids

The current grid convergence study uses the DPW-I standard structured overset grid and unstructured grid as part of the grid density study. Both of these standard grids were provided by the organizing committee and were built to the same grid specifications as defined by the organizing committee.[2] Additional grids (finer and coarser) were generated specifically for use in the current study.

Structured Overset Grids

The DPW-I standard overset grid (the medium grid in this study) was described fully in Ref. 9. It used near-field grids generated with hyperbolic marching,[25] embedded in intermediate and far-field cartesian box grids. The grid system contained a total of 3,727,462 grid points, with 3,231,377 non-blanked points and 54,445 surface grid points. The far-field boundary was 150 reference-chord lengths away from the surface. The workshop requirement was a minimum of 50 reference-chord lengths. Rumsey et al.[10] showed that grid extents of more than 25 reference-chord lengths away did not have a significant effect on the forces and moments for a transonic transport configuration. Grid connectivity for the DPW-I grid system was generated with the GMAN software.[26] Subsequent comparisons with grids assembled using PEGASUS 5 showed little change in global forces and moments. Figure 1 shows the wing/body surface mesh and symmetry plane for the workshop standard overset grid.

The chordwise spacing was set at the wing leading edge at approximately 0.10% of the local chord. The spacing at the trailing edge was approximately 0.12% of the local chord. The spacing at the tip was approximately 0.1% of the semi-span and at the root was approximately 1.0% of the semi-span. The wall normal spacing was set so that the first point off the wall was located at $y^+ \approx 1$. The maximum growth ratio in the wall normal direction was 1.24. The DPW-I geometry has a blunt trailing edge definition. The workshop overset-structured grid resolved the trailing edge with 4 cells. The wing trailing edge mesh had an underlying C-type topology that had additional resolution of the trailing-edge wake region.

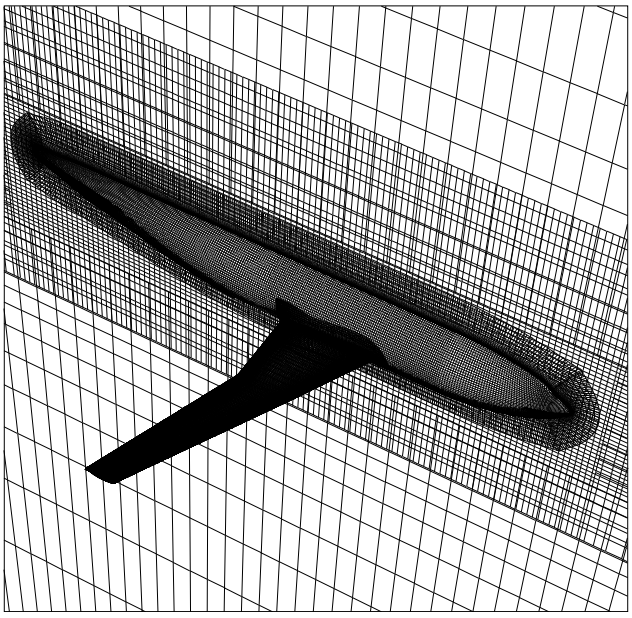

Fig. 1 DPW-I standard overset grid.

The coarse overset grid system was generated by taking every other point of the medium grid system. The wake of the wing tip cap grid was extended to more closely match the wake of the rest of the wing, ensuring enough overlap with the intermediate grid for adequate communication. This system contained 484,151 grid points (475,277 non-blanked).

To generate the fine overset grid system, parametric cubic interpolation was used in all three coordinate directions to insert midpoints between the existing grid points, starting with the medium grid system. Care was taken to maintain surface discontinuities, and simple linear interpolation was used at grid singularities. Some regions of the fine grids were smoothed to reduce distortion of the volume grid, specifically at the wing tip trailing edge. Again, the wake of the wing tip cap grid was extended downstream. The resulting grid system had 30,818,728 grid points, of which 28,630,101 were non-blanked. Table 1 compares the global grid sizes for the family of structured grids.

	Total Non-Blanked Cells	Boundary Cells	Trailing Edge Cells
Coarse	475,277	13,553	2
Medium	3,231,377	54,445	4
Fine	28,630,101	226,359	8

Table 1 Global grid size of structured grids.

Unstructured Grids

The DPW-I standard node-based grid was generated with the VGRIDns advancing-layer and advancing-front grid generation software package.[2,7] Figure 2 shows the wing/body surface mesh and symmetry plane for the workshop tetrahedral standard grid. The DPW-I standard grid was used for the coarse grid solution in the current grid convergence study. This grid contained a total of 1,647,810 vertices with 48,339 no-slip boundary vertices. The far-field boundary was 50 reference-chord lengths away from the surface. The chordwise grid spacing at the leading edge ranged from approximately 0.25% to 0.16% local chord. The chordwise grid spacing at the trailing edge was approximately 0.25% to 0.82% local chord. The maximum spanwise spacing was 0.4% semi-span at the leading edge and 0.6% semi-span at the trailing edge. The wall normal spacing was set so that the first point off the wall was located at $y^+ \approx 1$ (0.001 mm or 0.000708% of the reference chord). The clustering of points normal to the surface was computed according to the VGRIDns stretching function[7]

$$\delta_n = \delta_1[1 + r_1(1 + r_2)^{n-1}]^{n-1} \qquad (6)$$

where δ_n is the normal spacing of the n^{th} layer, δ_1 is the spacing of the first layer, and the factors r_1 and r_2 are constants that determine the rate of stretching. (Note if r_2 is zero the stretching is geometric.) For the workshop standard grid, r_1 and r_2 were 0.20 and 0.02, respectively. With these parameters, approximately 28 layers were present in the grid with a maximum growth of approximately 1.34. The workshop unstructured grid resolved the blunt trailing edge with 5 vertices. However, the mesh is restricted to an underlying O-type topology that had no additional resolution of the trailing-edge wake region.

A family of grids was designed for the grid convergence study such that the total number of the vertices in each mesh differ by a factor of approximately two between the coarse and medium grids and approximately three between the medium and fine mesh. The medium and fine grids were generated with VGRIDns by a global refinement of the spacing parameters (VGRIDns sourcing terms) used in the generation of the coarse grid of 0.75 and 0.5, respectively. The minimum wall spacing between the grids differs by a similar factor. Tables 2 and 3 compare the global grid sizes and grid generation parameters for the family of unstructured grids. The geometric growth in the boundary layer was modified for the medium and fine grids so that the geometric extent of the advancing layers was approximately the same in all the grids (see Table 2). The maximum growth rate in the advancing layers was 1.31 and 1.26 for the medium and fine grids, respectively. The blunt trailing edge was refined explicitly (see Table 3).

The grids generated with VGRIDns were fully tetrahedral. However, VGRIDns uses an advancing layer technique to generate the boundary layer portion of the grid so that prisms can be reconstructed in the boundary layer for use with NSU3D. The mixed-element grids have the same number of unknowns as the fully tetrahedral grids although the control volumes differ in the boundary layers.

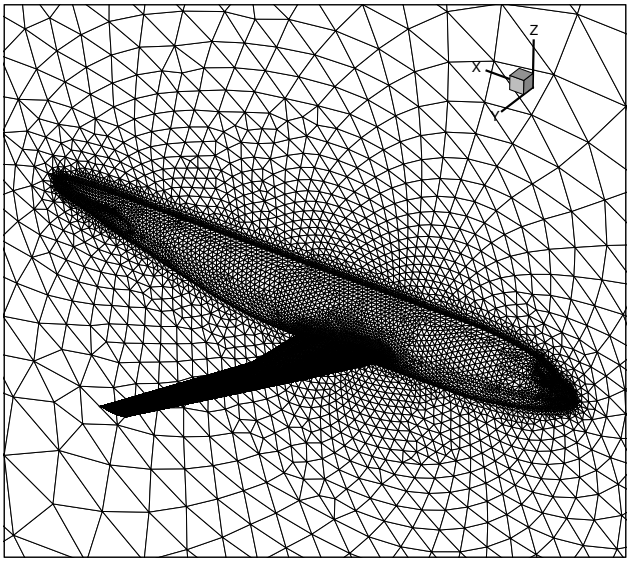

Fig. 2 DPW-I standard unstructured grid.

	δ_1 (mm)	r_1	r_2	Layers
Coarse	0.001	0.20	0.02	≈ 28
Medium	0.00075	0.17	0.02	≈ 31
Fine	0.00050	0.13	0.02	≈ 34

Table 2 Advancing-layer grid generation parameters for unstructured grids.

	Total Nodes	Boundary Nodes	Trailing Edge Nodes
Coarse	1,647,810	48,339	5
Medium	3,538,332	77,685	7
Fine	9,477,926	166,317	9

Table 3 Global grid size of unstructured grids.

Computational Results

DPW-I had two required cases for the participants. Case 1 was a transonic cruise condition at a constant lift, and Case 2 was a transonic drag polar at the same cruise Mach number. All cases were run at the test Reynolds number $Re_c = 3 \times 10^6$ based on geometric chord and were assumed to be fully turbulent.

Case 1 $M = 0.75$ $C_L = 0.500 \pm 0.001$
Case 2 $M = 0.75$ $\alpha = -3^\circ, -2^\circ, -1^\circ, 0^\circ, 1^\circ, 2^\circ$

The current study focused on Case 2 and in particular the $\alpha = 0^\circ$ angle-of-attack condition for the grid convergence study. For each of the codes, a "best" or "standard" practices method for executing the calculations was chosen. The configuration of each code is compared in Table 4 and is referred to as the baseline code configuration. TL1D refers to a thin-layer approximation in the wall-normal direction, TL3D refers to a thin-layer approximation in all directions, and FNS refers to full Navier-Stokes. CD refers to a central difference scheme with scalar dissipation (SD) or matrix dissipation (MD).

Code	Eq.	Diff. Scheme	Turb. Model
CFL3D	TL1D	Roe	SA
OVERFLOW	TL1D	CD/SD	SA+fv3
NSU3D	TL3D	CD/MD	SA
FUN3D	FNS	Roe	SA

Table 4 Baseline code configurations.

Workshop Required Transonic Polar

New Case 2 results computed with CFL3D and FUN3D on the workshop standard grids are compared to the OVERFLOW[9] and NSU3D[6] results reported at the workshop in Fig. 3. Experimental results[15] are also included in Fig. 3 for reference. (Recall the overset workshop standard grid is the medium structured grid, and the unstructured workshop standard grid is the coarse grid.) This figure shows the wing/body lift versus alpha curves, lift versus total drag curves and lift versus pitching moment curves. The lift versus alpha curves from the different codes compare well with each other over the lower range of angle of attack, but the results from NSU3D and FUN3D break early at the higher angles of attack. All codes over predict the experimental lift levels for most of the angle of attack range. Results from the four codes also compare well with each other for the drag polar at the lower angles of attack, with an increased variation at the higher angles of attack. The lift versus pitching moment curves show the largest code-to-code variation which increases at the higher angles of attack.

The range in drag predicted at $\alpha = 0^\circ$ was 14 counts between all four codes, 3 counts between the two structured grid codes, and 6 counts between the two unstructured grid codes. The corresponding range of lift at $\alpha = 0^\circ$ was 0.021 between all four codes, 0.003 between the two structured grid codes, and 0.016 between the two unstructured grid codes. The range of lift in terms of percent of the cruise lift ($C_L = 0.500$) is 4.2% between all four codes. Based on a population of the four results

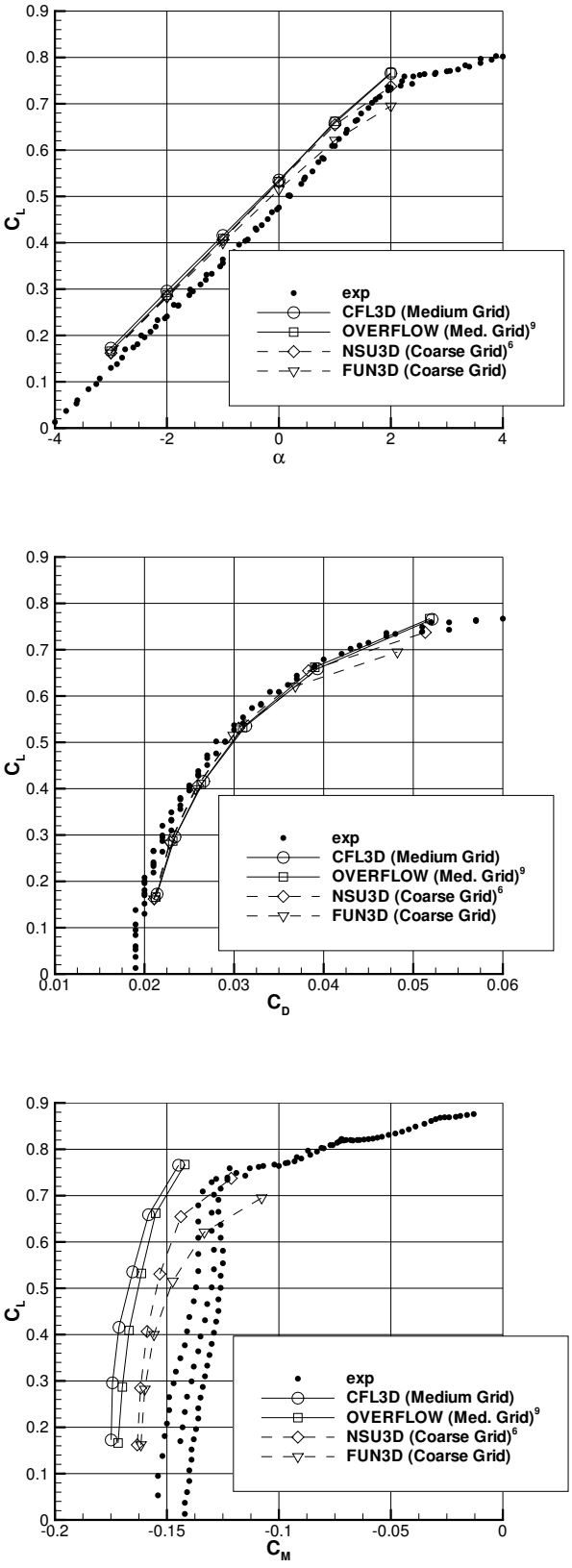

Fig. 3 Comparison of force and moment results at $M = 0.75$ from the DPW-I standard grids.

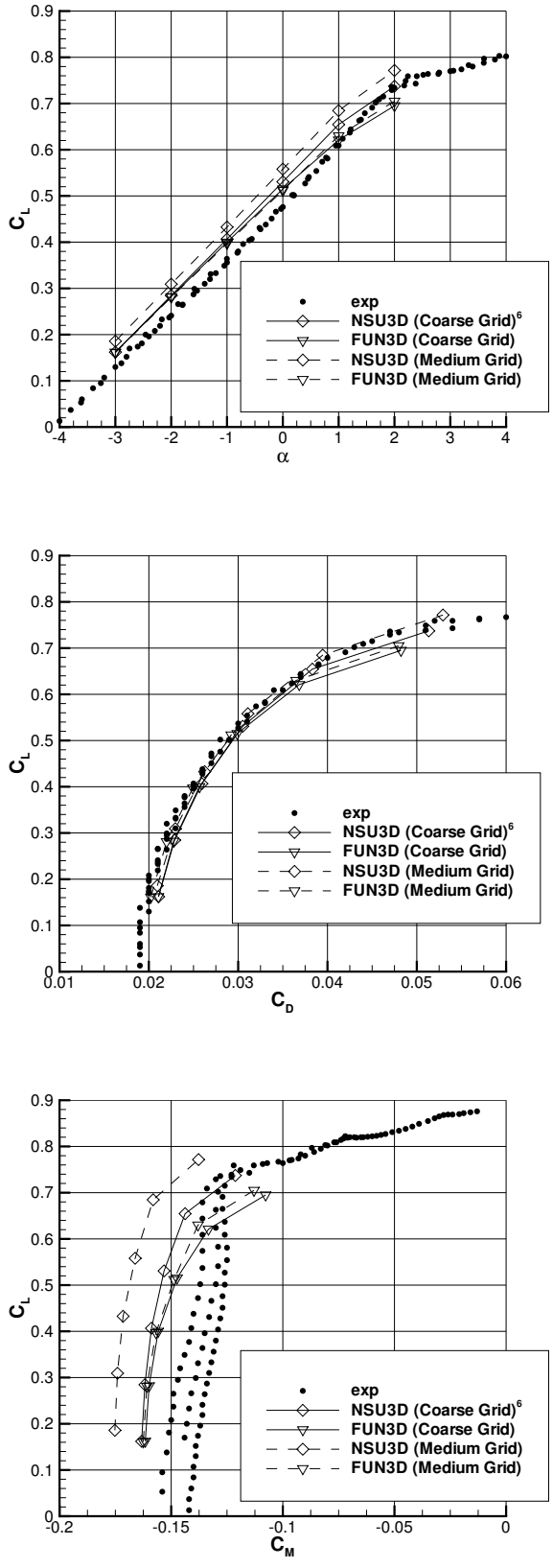

Fig. 4 Comparison of force and moment results at $M = 0.75$ from the coarse and medium unstructured grids.

computed on the workshop standard grids, the mean drag at $\alpha = 0°$ was 0.03067 and the variation in terms of standard deviation was 6 counts.

Grid Convergence Study

Force and moment results computed on the medium unstructured grid are compared in Fig. 4 to the unstructured coarse (workshop) grid results to show the effect of unstructured grid refinement on the polar solutions. At each angle of attack, there was an *increase* in variation of forces and moment between the two unstructured grid codes as the grid was refined. The range in drag increased from 6 counts to 19 counts at $\alpha = 0°$, and the range of lift increased from 0.016 (3.2%) to 0.047 (9.4%). This result was unexpected; generally the expectation is that variation between codes should decrease as the grid density is increased. The possible causes of the reverse trend seen in this study will be explored further below.

The $M = 0.75$, $\alpha = 0°$ angle of attack case was computed on the coarse, medium and fine structured and unstructured grids for all codes in their baseline configuration (with one exception: CFL3D was unable to complete its computation on the fine grid given the time and resources available). It should be noted that the OVERFLOW solution on the fine grid was not completely converged; even after nearly 20,000 multi-grid cycles, the results showed an oscillatory trend in the residual histories, forces and moments. In spite of the lack of satisfactory convergence for this case, "average" force and moment values were extracted and presented that are believed to be approximately correct based on trend analysis, to within roughly 0.004 in lift coefficient, 0.0003 in drag coefficient, and 0.002 in moment coefficient. Table 5 shows a summary of all $M = 0.75$, $\alpha = 0°$ cases run in this study.

Figures 5 - 9 show the lift, total drag, pressure drag, viscous drag and pitching moment versus $N^{-2/3}$, where N is the number of cells for structured grids and vertices for unstructured grids. (In the asymptotic range, one would expect an approximate linear variation in forces or moments with $N^{-2/3}$ for a second order scheme.) Thus, results using finer grids appear to the left in the figures, and results using coarser grids appear to the right. There are also additional CFL3D and OVERFLOW data points on these plots for solutions on the medium structured grid which were computed with different thin-layer approximations than the baseline.

Overall, these figures show that as the grids are refined from coarse to medium on the structured grids, the variation between codes decreases as expected. But as the unstructured grids are refined, the variation generally increases. For example, in comparing the NSU3D and FUN3D results, the total drag range increased with grid

Code	Eq.	Diff. Scheme	Turb. Model	Mesh	C_L	C_D	C_{Dp}	C_{Dv}	C_M
CFL3D	TL1D	Roe	SA	Coarse	0.514	0.02576	0.01273	0.01303	-0.1626
CFL3D[9]	TL1D	Roe	SA	Medium	0.535	0.03130	0.01763	0.01367	-0.1653
CFL3D	TL3D	Roe	SA	Medium	0.539	0.03144	0.01779	0.01367	-0.1662
Overflow	TL1D	CD/SD	SA+fv3	Coarse	0.463	0.03525	0.01990	0.01535	-0.1491
Overflow	TL1D	Roe	SA+fv3	Coarse	0.554	0.02912	0.01489	0.01423	-0.1623
Overflow[9]	TL1D	CD/SD	SA+fv3	Medium	0.532	0.03097	0.01719	0.01378	-0.1614
Overflow	TL3D	CD/SD	SA+fv3	Medium	0.522	0.03095	0.01723	0.01372	-0.1589
Overflow	FNS	CD/SD	SA+fv3	Medium	0.504	0.03114	0.01741	0.01374	-0.1531
Overflow	TL1D	Roe	SA+fv3	Medium	0.527	0.03064	0.01705	0.01360	-0.1608
Overflow*	TL1D	CD/SD	SA+fv3	Fine	0.532	0.02977	0.01662	0.01315	-0.1630
NSU3D[6]	TL3D	CD/MD	SA	Coarse	0.531	0.03051	0.01817	0.01233	-0.1532
NSU3D	TL3D	CD/MD	SA	Medium	0.558	0.03109	0.01825	0.01284	-0.1661
NSU3D	TL3D	CD/MD	SA	Fine	0.558	0.03078	0.01770	0.01308	-0.1673
FUN3D	FNS	Roe	SA	Coarse	0.514	0.02989	0.01774	0.01215	-0.1473
FUN3D	FNS	Roe	SA	Medium	0.511	0.02920	0.01701	0.01219	-0.1487
FUN3D	FNS	Roe	SA	Fine	0.501	0.02860	0.01648	0.01212	-0.1465

* Oscillatory trend in convergence history.

Table 5 Summary of $M = 0.75$, $\alpha = 0^\circ$ Results.

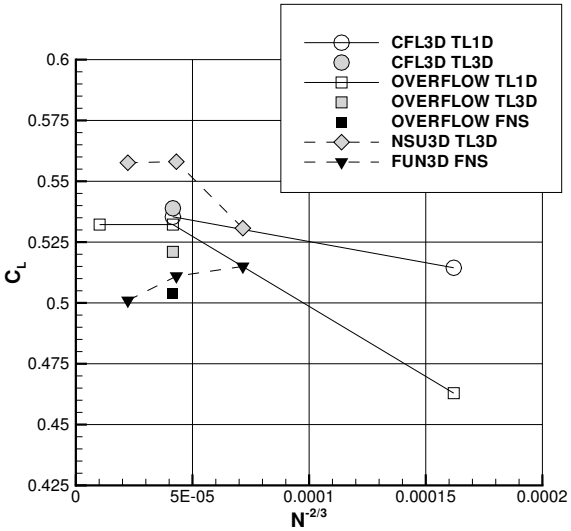

Fig. 5 Comparison of lift versus number of cells or vertices to the -2/3 power at $M = 0.75$, $\alpha = 0^\circ$.

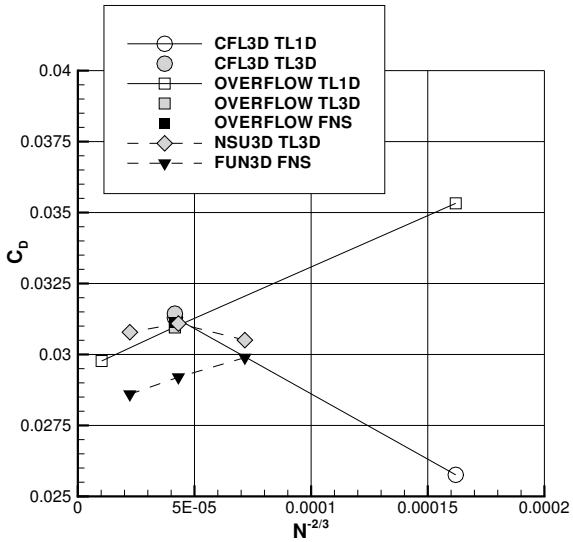

Fig. 6 Comparison of total drag versus number of cells or vertices to the -2/3 power at $M = 0.75$, $\alpha = 0^\circ$.

refinement from 6 counts on the coarse grid to 19 counts on the medium grid to 22 counts on the fine grid. The pressure drag and viscous drag components also show an increase in range with grid refinement. The pressure drag range increased with grid refinement from 5 counts on the coarse grid to 13 counts on the medium grid but decreased slightly to 12 counts on the fine grid. The viscous drag range increased with grid refinement from 1 count on the coarse grid to 6 counts on the medium grid to 10 counts on the fine grid. The range in lift increased from 0.016 on the coarse grid to 0.047 on the medium grid to 0.057 on the fine grid. The range of lift in terms of percent of the cruise lift $C_L = 0.500$ increased from 3.2% to 9.4% to 11.4%.

Figure 10 shows the grid convergence of the surface pressure coefficient at one span station located near the wing-root juncture and one span station just outboard of the the wing break. These two pressure distributions indicate two of the relevant flow features at this angle of attack: a separation bubble near the trailing edge of the wing-root juncture and a mild normal shock across the span of the wing near the quarter chord. A comparison

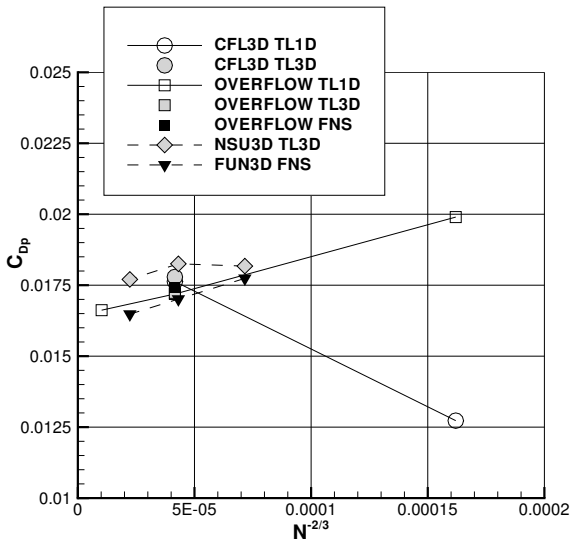

Fig. 7 Comparison of pressure drag versus number of cells or vertices to the -2/3 power at $M = 0.75$, $\alpha = 0^\circ$.

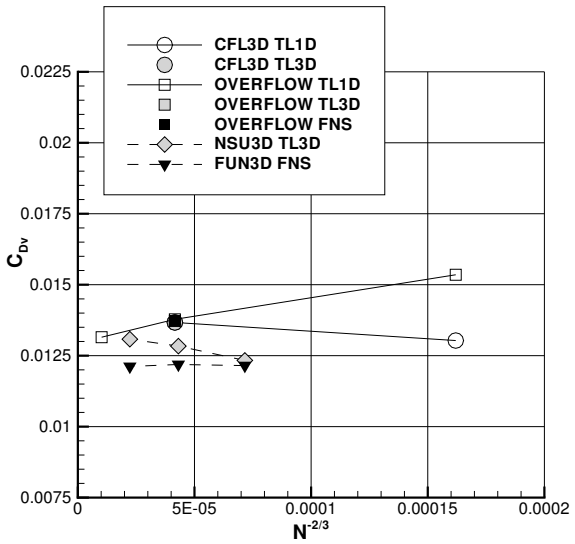

Fig. 8 Comparison of viscous drag versus number of cells or vertices to the -2/3 power at $M = 0.75$, $\alpha = 0^\circ$.

of surface restricted streamlines shown later in the paper show that differences in the inboard pressure distribution are indicative of differences in the wing-root juncture separation.

First, we examine the structured grid results in detail. Comparing results in Fig. 10, it is seen that CFL3D exhibits only minor differences between results on the coarse and medium grids, whereas OVERFLOW exhibits very large differences. On the coarse grid, OVERFLOW predicted a significantly larger wing-root juncture separation compared to the other solutions and the spanwise shock was excessively smeared. Fig. 11 compares surface streamlines between CFL3D and OVERFLOW on

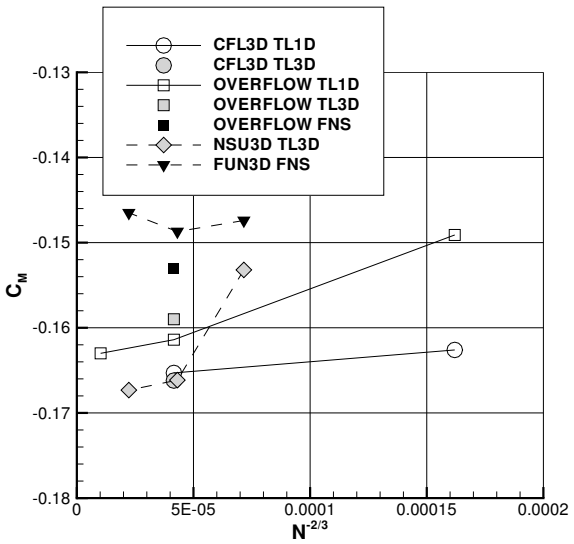

Fig. 9 Comparison of pitching moment versus number of cells or vertices to the -2/3 power at $M = 0.75$, $\alpha = 0^\circ$.

the medium grid, and Fig. 12 shows similar results on the coarse grid. These figures show the relative sizes of the wing-root juncture separation bubble. OVERFLOW with CD/SD exhibits more grid sensitivity between these two grids. On the other hand, OVERFLOW's fine grid result showed only small differences from its medium grid result (no fine grid result was available for CFL3D). These large differences between CFL3D and OVERFLOW on the coarse grid translate into the large variations in forces and moments seen in Figs. 5 - 9.

Considering the structured grid results in Figs. 5 - 9, it is difficult to discern trends with confidence. For OVERFLOW, the coarse grid produces a solution very different in character from finer grid results, so it clearly lies outside of the asymptotic range. For CFL3D, a fine grid result was not attainable due to resource constraints, so its trend is also unclear. The difficulties encountered in this grid refinement study using the overset structured grids reinforces the assertion of Roache in Ref. 4 that grid doubling, although preferable, may not be practical for three-dimensional problems due to the fact that the fine grid is often too expensive to calculate and the coarse grid is out of the asymptotic range.

Next, we examine the unstructured grid results in more detail. The NSU3D coarse, medium and fine grid results in Figs. 5 - 9 indicate that the coarse grid solution is not in the asymptotic range of convergence. A comparison of chordwise pressure distributions for the NSU3D solutions in Fig. 10 shows that the flowfield in the area of wing-root juncture separation changes very little with coarse to medium grid refinement while the spanwise shock strengthens and moves aft. The increased loading and shift in shock location corresponds to the increase in lift and drag and the decrease in pitching moment shown

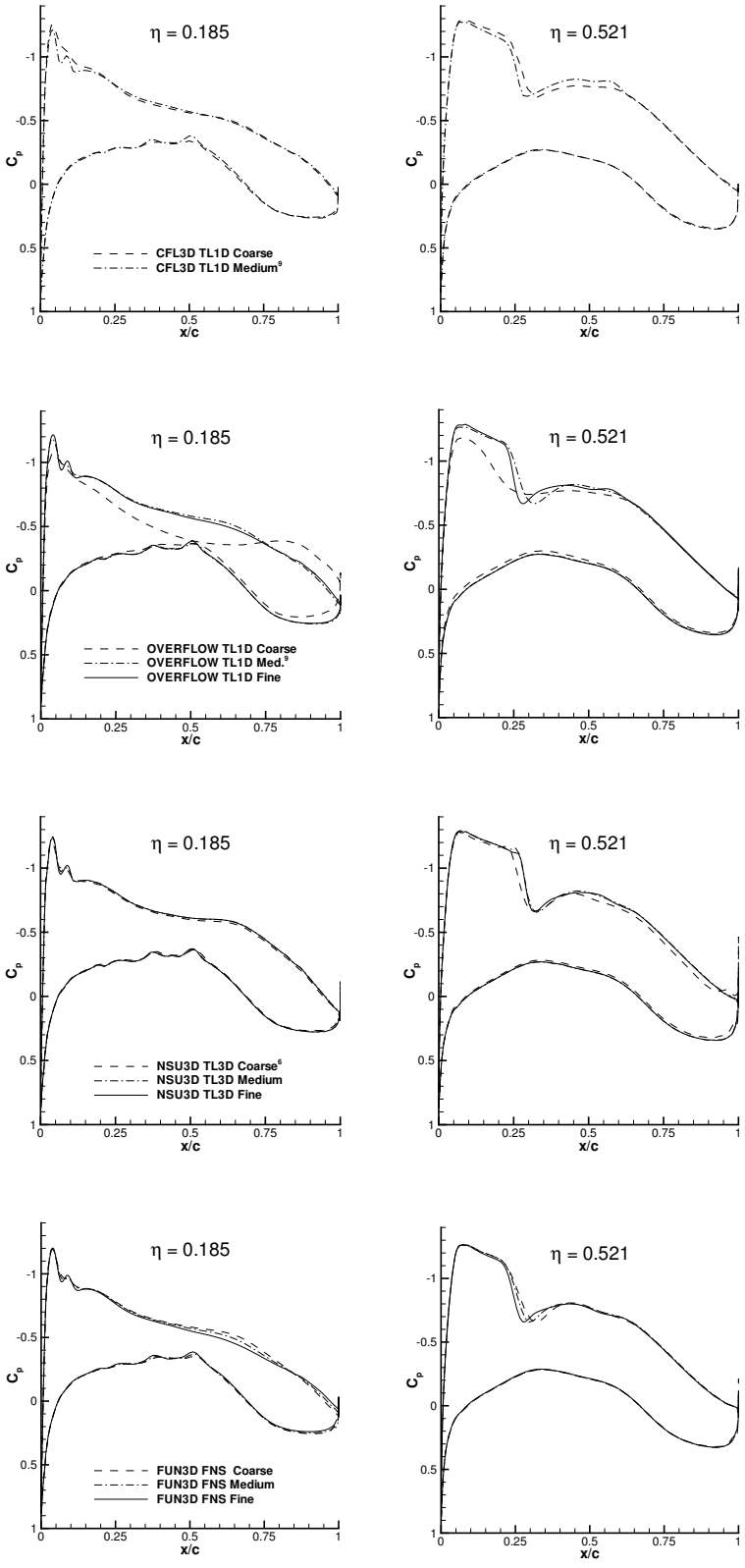

Fig. 10 Grid convergence of chordwise pressure distributions at $M = 0.75$, $\alpha = 0^\circ$.

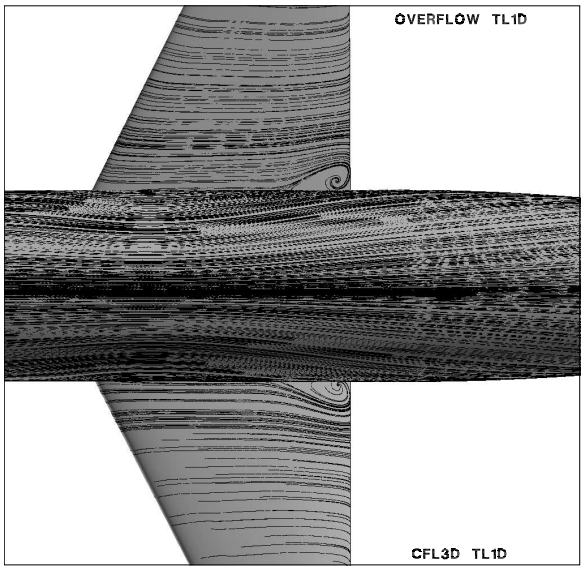

Fig. 11 Comparison of surface restricted streamlines for medium structured grids.

Fig. 12 Comparison of surface restricted streamlines for coarse structured grids.

in Figs. 5 - 9. Figure 10 also indicates very small changes in the chordwise pressure distributions with medium to fine grid refinement for the NSU3D solutions, which corresponds to the small variations noted in the computed forces and moment.

The FUN3D coarse, medium and fine grid results in Figs. 5 - 9 indicate that the three solutions may lie within the asymptotic range of convergence in terms of drag, but the lift and moment do not plot as straight lines. A comparison of chordwise pressure distributions for the FUN3D solutions in Fig. 10 indicates that the area of wing-root juncture separation increased with grid refinement as the spanwise shock strengthened and moved forward. The decreased loading due to increased separation and shock motion corresponds to the decrease in lift and drag with grid refinement shown in Figs. 5 - 8. The pitching moment variation shown in Fig. 9 does not vary monotonically with grid refinement which may indicate that although there is a loss in lift, there is a compensating shift in loading. A comparison of surface streamlines in Fig. 13 shows the relative sizes of the wing-root juncture separation between the NSU3D and FUN3D medium grid results. Note that the small amount of separation predicted by NSU3D (approximately 1.4% of the wing semi-span) is obscured by the fuselage in the planform view.

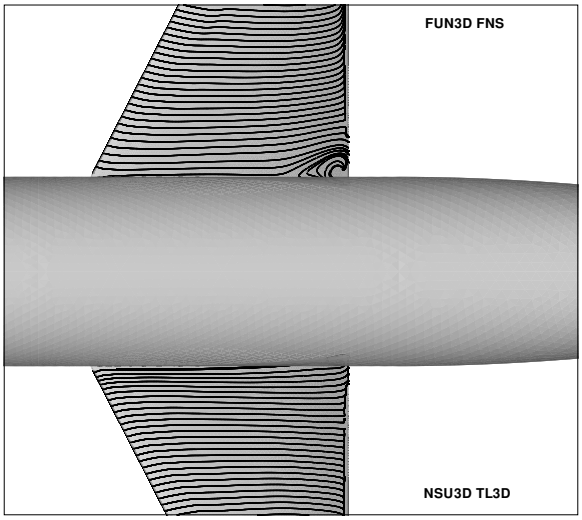

Fig. 13 Comparison of surface restricted streamlines from FUN3D and NSU3D medium grid results.

Effects of Numerical Implementations

In an effort to try to determine a possible cause for the trend of increasing variation between unstructured code results as the grids are refined, the effects of the thin-layer approximation and difference schemes were investigated. Recall that the "baseline" methods for each of the codes is: TL1D for CFL3D and OVERFLOW, TL3D for NSU3D, and FNS for FUN3D (refer to Table 4). In terms of thin-layer approximations versus full Navier-Stokes, neither NSU3D nor FUN3D could be run using methods other than their baseline. However, CFL3D has the capability to use either TL1D or TL3D and OVERFLOW can use TL1D, TL3D, or FNS. Therefore, on the medium grids these options were exercised to determine their effect. In Figs. 5 - 9, it is seen that there is very little difference between CFL3D with TL1D and TL3D. OVERFLOW, on the other hand, exhibits significant differences in lift (which successively decreases for TL3D and FNS) and pitching moment (which successively increases for TL3D and FNS). For example, the lift decreases from $C_L = 0.532$ for TL1D to $C_L = 0.522$

for TL3D to $C_L = 0.504$ for FNS. It is interesting to note that this trend is consistent with the fact that FUN3D (FNS) yields lower lift levels and higher moment levels than NSU3D (TL3D). However, the drag computed with OVERFLOW does not vary significantly between TL1D and FNS and is still high in comparison with the FUN3D medium grid results.

Figure 14 shows surface pressure coefficients on the medium level grids using the four codes' baseline methods, along with the OVERFLOW result using FNS. In going from TL1D to FNS, OVERFLOW predicts the shock location to be further forward, and also exhibits a significant difference (more separation) at the inboard station where the separation bubble is located. A comparison of surface streamlines for the OVERFLOW TL1D and FNS results in Fig. 15 also confirms the increase separation predicted with the FNS.

Unfortunately, it is impossible to draw any firm conclusions from this part of the study. Several questions remain unanswered. It is unclear from the current results why OVERFLOW exhibit a significant difference between TL1D and TL3D but CFL3D does not. This inconsistency could be related to the fact that OVERFLOW used central differencing and CFL3D used upwind differencing. A comparison of Roe upwind results from OVERFLOW calculations on the coarse and medium grids is shown in Table 5. On the coarse grid, the effects of Roe upwind versus central differences on lift and drag is significant, and the variation between the CFL3D and OVERFLOW results is decreased from the baseline results. However, on the medium grid the effect of upwind differences is much smaller, and the variation between CFL3D and OVERFLOW results is slightly increased.

Although the trend between OVERFLOW's TL3D to FNS was consistent with the variation between NSU3D and FUN3D, there appears to be some differences not accounted for. For example, drag results from FUN3D were lower than that of NSU3D and the other codes. Drag results from OVERFLOW did not exhibit the same trend. Also, the shock location predicted by NSU3D at the outboard stations was further downstream from the shock location predicted by the other codes. Finally, OVERFLOW FNS results showed more separation at the wing-root juncture than FUN3D which is also FNS.

Conclusions

Calculations on the DPW-I DLR-F4 wing-body were made with four CFD codes commonly used at NASA Langley Research Center. Forces and moments were computed on the DPW-I workshop standard structured overset and unstructured grids, and the results were compared for the required transonic drag polar case. The range in total drag predicted for the workshop standard grids at $\alpha = 0^\circ$ was 14 counts. The variation of drag in terms of standard deviation was 6 counts.

Additional calculations at $\alpha = 0^\circ$ were performed on the two families of structured and unstructured grids to evaluate the variation in forces and moments with grid refinement. On the fine overset structured grid, OVERFLOW results were not completely converged, and the CFL3D results were not completed due to slow convergence and resource constraints. The CFL3D and OVERFLOW coarse grid solutions were not of sufficient resolution to be used to accurately quantify the variation in forces and moments due to grid refinement. The difficulties encountered in the structured grid refinement study reinforced the issues concerning the impracticality of using grid doubling in each direction for three-dimensional problems.

The grid refinement study for the node-based unstructured grid codes, NSU3D and FUN3D, showed an increase in code-to-code variation of forces and moments with grid refinement. The total drag difference of 6 counts, 19 counts and 22 counts was observed on the coarse (workshop), medium and fine grids, respectively. However, the results were not definitively in the range of asymptotic grid convergence. A comparison of grid convergence in chordwise pressure distributions for the structured and unstructured grid codes indicated that some solutions are converged to different shock locations and root-juncture flow separation patterns. Additional structured grid results on the medium grid indicated a possible effect due to thin-layer approximations. Overall, the current grid convergence study was inconclusive in determining if the increased variation in forces and moments was due to discretization errors or modeling differences between the codes.

In spite of its inconclusive nature, this study exemplified the difficulties inherent in conducting a definitive grid convergence study for three-dimensional aerodynamic configurations. By using only a single CFD code, one can sometimes be misled into believing that results lie in the asymptotic range and that results are representative of the "correct" answer. Clearly, there are more factors that need to be considered, as this study using four different CFD codes demonstrated. It appears that certain numerical schemes (central vs. upwind, thin vs. full) or other code-to-code differences may have a larger effect than previously thought on grid sizes considered to be "medium" or "fine" by today's standards. Whether this effect diminishes for even finer grids lies beyond current routine capabilities, and remains to be examined at some time in the future.

Acknowledgments

The authors would like to thank Dr. Shahyar Pirzadeh of NASA Langley Research Center for providing VGRIDns version 3.5 and the standard grid DLR-F4 restart files

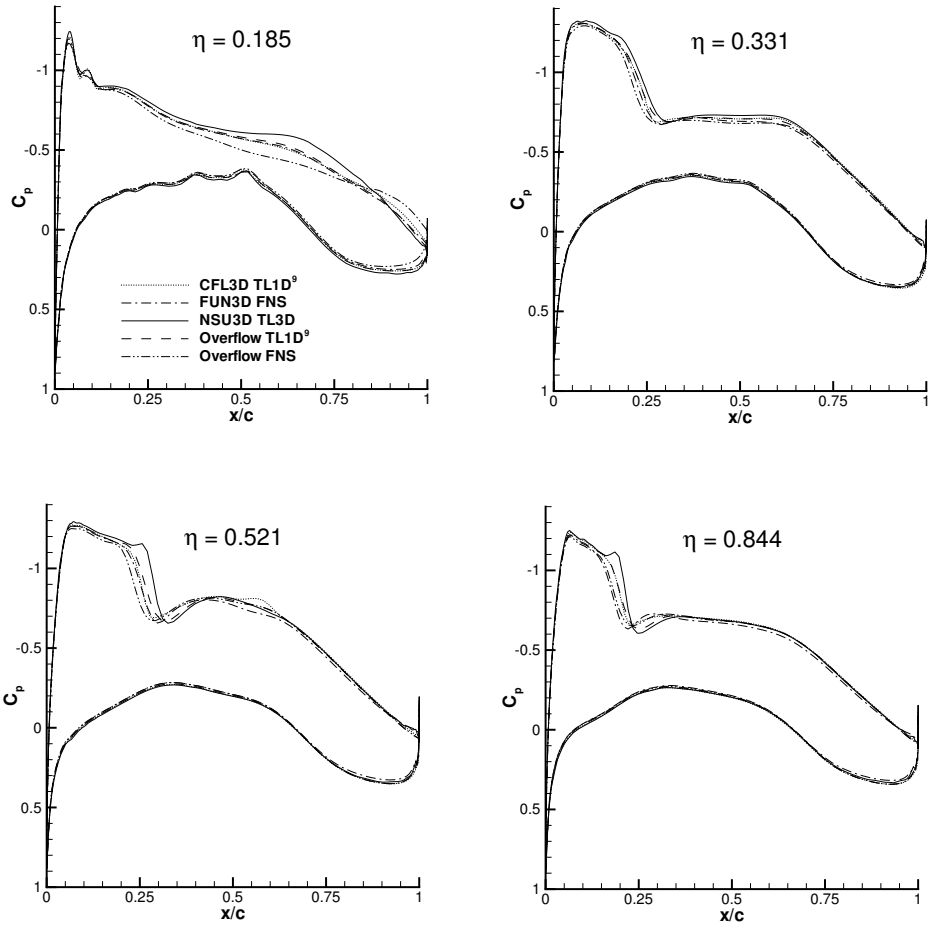

Fig. 14 Comparison of surface pressure distributions for medium grids.

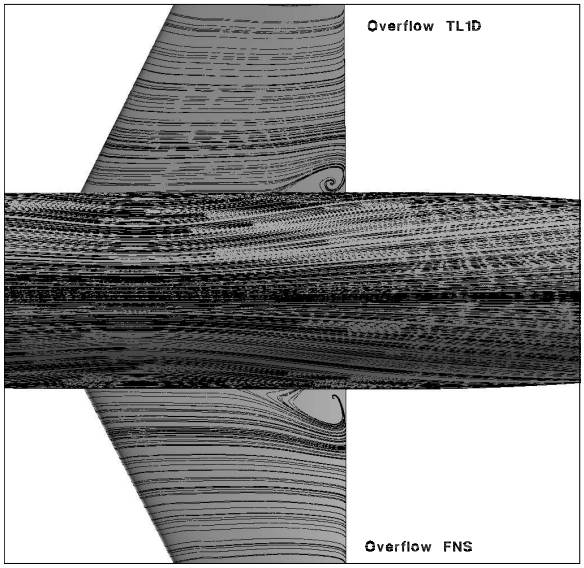

Fig. 15 Comparison of surface restricted streamlines from OVERFLOW medium grid results.

for use in generating the medium and fine unstructured grids for this study. The authors would also like to thank Mr.Reynaldo Gomez of NASA Johnson Spaceflight Center for supplying the coarse overset grid and Dr. Eric Nielsen of NASA Langley Research Center for his expert advice in support of the FUN3D calculations.

References

[1]Redeker, G., Muller, R., Ashill, P. R., Elsenaar, A., and Schmitt, V., "Experiments on the DLR-F4 Wing Body Configuration in Several European Wind Tunnels," Tech. Rep. AGARD CP-429, Jul. 1988.

[2]Levy, D. W., Zickuhr, T., Vassberg, J., Agrawal, S., Wahls, R. A., Pirzaheh, S., and Hemsch, M. J., "Summary of Data from the First AIAA CFD Drag Prediction Workshop," Tech. Rep. AIAA-2002-0841, Jan. 2002.

[3]Hemsch, M. J., "Statistical Analysis of CFD Solutions from the Drag Prediction Workshop," Tech. Rep. AIAA-2002-0842, Jan. 2002.

[4]Roache, P. J., *Verification and Validation in Computational Science and Engineering*, Hermosa Publishers, 1998.

[5]Rakowitz, M., Eisfeld, B., Schwamborn, D., and Sutcliffe, M., "Structured and Unstructured Computations on the DLR-F4 Wing-Body Configuration," *Journal of Aircraft*, Vol. 40, No. 2, Mar. 2003, pp. 256–264.

[6]Mavriplis, D. J. and Levy, D. W., "Transonic Drag Prediction Using an Unstructured Multigrid Solver," Tech. Rep. AIAA-2002-0838, Jan. 2002.

[7]Pirzadeh, S. Z. and Frink, N. T., "Assessment of the Unstructured Grid Software TetrUSS for Drag Prediction of the DLR-F4 Configuration," Tech. Rep. AIAA-2002-0839, Jan. 2002.

[8]Rumsey, C. L. and Biedron, R. T., *Computation of Flow Over a Drag Prediction Workshop Wing/Body Transport Configuration Using CFL3D*, NASA/TM-2001-211262, 2001.

[9]Vassberg, J., Buning, P. G., and Rumsey, C. L., "Drag Prediction for the DLR-F4 Wing/Body using OVERFLOW and CFL3D on an Overset Mesh," Tech. Rep. AIAA-2002-0840, Jan. 2002.

[10]Rumsey, C. L., Allison, D. O., Biedron, R. T., Buning, P. G., Gainer, T. G., Morrison, J. H., Rivers, M., Mysko, S. J., and Witkowski, D. P., *Sensitivity Analysis of a Modern Civil Transport Near Buffet-Onset Conditions*, NASA TM-2001-211263, 2001.

[11]Krist, S. L., Biedron, R. T., and Rumsey, C. L., *CFL3D User's Manual (Version 5.0)*, NASA TM-1998-208444, 1998.

[12]Jespersen, D. C., Pulliam, T. H., and Buning, P. G., "Recent Enhancements to OVERFLOW," Tech. Rep. AIAA-97-0644, Jan. 1997.

[13]Mavriplis, D. J. and Venkatakrishnan, V., "A Unified Multigrid Solver for the Navier-Stokes Equations on Mixed Element Meshes," *International Journal for Computational Fluid Dynamics*, , No. 8, 1997, pp. 247–263.

[14]Anderson, W. K., Rausch, R. D., and Bonhaus, D. L., "Implicit/Multigrid Algorithms for Incompressible Turbulent Flows on Unstructured Grids," *Journal of Computational Physics*, Vol. 128, No. 2, 1996, pp. 391–408.

[15]Redeker, G., "DLR-F4 Wing-Body Configuration In A Selection of Experimental Test Cases for the Validation of CFD Codes," Tech. Rep. AGARD AR-303, Aug. 1994.

[16]Roe, P. L., "Approximate Riemann Solvers, Parameter Vectors, and Difference Schemes," *Journal of Computational Physics*, Vol. 43, 1981, pp. 357–372.

[17]Buning, P. G., Jespersen, D. C., Pulliam, T. H., Klopfer, G. H., Chan, W. M., Slotnick, J. P., Krist, S. E., and Renze, K. J., *OVERFLOW User's Manual (Version 1.8s)*, 2000.

[18]Jameson, A., Schmidt, W., and Turkel, E., "Numerical Solution of the Euler Equations by Finite Volume Methods Using Runge-Kutta Time Stepping Schemes," Tech. Rep. AIAA-81-1259, 1981.

[19]Suhs, N. E., Rogers, S. E., and Dietz, W. E., "PEGASUS 5: An Automated Pre-Processor for Overset-Grid CFD," Tech. Rep. AIAA-2002-3186, Jun. 2002.

[20]Anderson, W. K. and Bonhaus, D. L., "An Implicit Upwind Algorithm for Computing Turbulent Flows on Unstructured Grids," *Computers and Fluids*, Vol. 23, No. 1, 1994, pp. 1–22.

[21]Nielsen, E. J., *Aerodynamic Design Sensitivities on an Unstructured Mesh Using the Navier-Stokes Equations and a Discrete Adjoint Formulation*, Ph.D. thesis, Virginia Polytechnic Institute and State University, 1998.

[22]Nielsen, E. J., "An Exact Dual Discrete Adjoint Solution Method for Turbulent Flows on Unstructured Grids," Tech. Rep. AIAA-2003-0272, Jan. 2003.

[23]Mavriplis, D. J., "Multigrid Strategies for Viscous Flow Solvers on Anisotrpic Unstructured Meshes," *Proceedings of the 13th AIAA CFD Conference, Snowmass, CO*, Jun. 1997, pp. 659–675, AIAA Paper 97-1952-CP.

[24]Spalart, P. R. and Allmaras, S. R., "A One-Equation Turbulence Model for Aerodynamic Flows," *La Recherche Aerospatiale*, , No. 1, 1994, pp. 5–21.

[25]Chan, W. M., Buning, P. G., and Chiu, I. T., *User's Manual for the HYPGEN Hyperbolic Grid Generator and the HGUI Graphical User Interface*, NASA TM-1993-108791, 1993.

[26]Gatzke, T. D., LaBozzetta, W. F., Frinfrock, G. P., Johnson, J. A., and Romer, W. W., "MACGS: A Zonal Grid Generation System for Complex Aero-Propulsion Configurations," Tech. Rep. AIAA-1991-2156, Jun. 1991.